



Since January 2020 Elsevier has created a COVID-19 resource centre with free information in English and Mandarin on the novel coronavirus COVID-19. The COVID-19 resource centre is hosted on Elsevier Connect, the company's public news and information website.

Elsevier hereby grants permission to make all its COVID-19-related research that is available on the COVID-19 resource centre - including this research content - immediately available in PubMed Central and other publicly funded repositories, such as the WHO COVID database with rights for unrestricted research re-use and analyses in any form or by any means with acknowledgement of the original source. These permissions are granted for free by Elsevier for as long as the COVID-19 resource centre remains active.



Contents lists available at ScienceDirect

Journal of Controlled Release

journal homepage: www.elsevier.com/locate/jconrel

Inhibition of SARS-CoV-2 replication in the lung with siRNA/VIPER polyplexes

Domizia Baldassi^a, Shubhankar Ambike^b, Martin Feuerherd^b, Cho-Chin Cheng^b, David J. Peeler^c, Daniel P. Feldmann^d, Diana Leidy Porrás-González^e, Xin Wei^e, Lea-Adriana Keller^{a,f}, Nikolaus Kneidinger^g, Mircea Gabriel Stoleriu^h, Andreas Popp^f, Gerald Burgstaller^e, Suzie H. Pun^c, Thomas Michler^{b,i}, Olivia M. Merkel^{a,e,*}

^a Department of Pharmacy, Pharmaceutical Technology and Biopharmaceutics, Ludwig-Maximilians-University of Munich, Butenandtstraße 5, 81377 Munich, Germany

^b Institute of Virology, School of Medicine, Technical University of Munich / Helmholtz Zentrum Munich, Trogerstr.30, 81675 Munich, Germany

^c Department of Bioengineering and Molecular Engineering and Sciences Institute, University of Washington, Seattle, WA, United States

^d Department of Oncology, Wayne State University School of Medicine, 4100 John R St, Detroit, MI 48201, United States

^e Institute of Lung Health and Immunity (LHI) and Comprehensive Pneumology Center (CPC) with the CPC-M bioArchive, Helmholtz Munich, Member of the German Center for Lung Research (DZL), Munich, Germany

^f Preclinical Safety, AbbVie Deutschland GmbH & Co. KG, Knollstrasse, 67061 Ludwigshafen, Germany

^g Department of Medicine V, University Hospital, LMU, Munich, Member of the German Center for Lung Research (DZL), Germany

^h Center for Thoracic Surgery Munich, Ludwig-Maximilians-University of Munich (LMU) and Asklepios Pulmonary Hospital; Marchioninistraße 15, 81377 Munich and Robert-Koch-Allee 2, 82131 Gauting, Germany

ⁱ Institute of Laboratory Medicine, University Hospital, LMU, Munich, Germany

ARTICLE INFO

Keywords:

siRNA delivery
RNA therapeutics
SARS-CoV-2
Pulmonary delivery
Human precision-cut lung slices

ABSTRACT

SARS-CoV-2 has been the cause of a global pandemic since 2019 and remains a medical urgency. siRNA-based therapies are a promising strategy to fight viral infections. By targeting a specific region of the viral genome, siRNAs can efficiently downregulate viral replication and suppress viral infection. However, to achieve the desired therapeutic activity, siRNA requires a suitable delivery system. The VIPER (virus-inspired polymer for endosomal release) block copolymer has been reported as promising delivery system for both plasmid DNA and siRNA in the past years. It is composed of a hydrophilic block for condensation of nucleic acids as well as a hydrophobic, pH-sensitive block that, at acidic pH, exposes the membrane lytic peptide melittin, which enhances endosomal escape. In this study, we aimed at developing a formulation for pulmonary administration of siRNA to suppress SARS-CoV-2 replication in lung epithelial cells. After characterizing siRNA/VIPER polyplexes, the activity and safety profile were confirmed in a lung epithelial cell line. To further investigate the activity of the polyplexes in a more sophisticated cell culture system, an air-liquid interface (ALI) culture was established. siRNA/VIPER polyplexes reached the cell monolayer and penetrated through the mucus layer secreted by the cells. Additionally, the activity against wild-type SARS-CoV-2 in the ALI model was confirmed by qRT-PCR. To investigate translatability of our findings, the activity against SARS-CoV-2 was tested *ex vivo* in human lung explants. Here, siRNA/VIPER polyplexes efficiently inhibited SARS-CoV-2 replication. Finally, we verified the delivery of siRNA/VIPER polyplexes to lung epithelial cells *in vivo*, which represent the main cellular target of viral infection in the lung. In conclusion, siRNA/VIPER polyplexes efficiently delivered siRNA to lung epithelial cells and mediated robust downregulation of viral replication both *in vitro* and *ex vivo* without toxic or immunogenic side effects *in vivo*, demonstrating the potential of local siRNA delivery as a promising antiviral therapy in the lung.

* Corresponding author at: Department of Pharmacy, Pharmaceutical Technology and Biopharmaceutics, Ludwig-Maximilians-University of Munich, Butenandtstraße 5, 81377 Munich, Germany.

E-mail address: olivia.merkel@lmu.de (O.M. Merkel).

<https://doi.org/10.1016/j.jconrel.2022.03.051>

Received 15 January 2022; Received in revised form 24 March 2022; Accepted 27 March 2022

Available online 29 March 2022

0168-3659/© 2022 Elsevier B.V. All rights reserved.

1. Introduction

In 2019, the severe acute respiratory syndrome coronavirus-2 (SARS-CoV-2) triggered the Covid-19 pandemic that resulted in dramatic consequences on health, politics and economics on a global scale. As of December 2021, 274 million cases were registered worldwide, and over 5 million people have died due to the consequences of viral infection [1]. SARS-CoV-2 is transmitted through respiratory secretions [2] and replicates primarily in respiratory epithelial cells [3]. In severe cases, the disease can lead to lung failure and death, especially in patients with pre-existing lung or cardiovascular diseases [4]. Although different approaches are now available to fight Covid-19, it still represents an unmet medical need. In the last year, a number of vaccines has been approved by FDA and EMA for clinical use, two of which are based on mRNA technology [5,6]. Although the introduction of vaccines has led to huge improvements in the battle against COVID-19, the pandemic is still far from an end at the time of writing this manuscript. Some antiviral drugs have been repurposed in the treatment of SARS-CoV-2 infection, such as the RNA polymerase inhibitor Remdesivir, but none of them can be considered satisfactory for the treatment of the disease [7]. Only recently two novel oral antiviral therapies have been approved [8,9]. The development of novel antiviral drugs is especially challenging in the case of coronaviruses as they use cellular components to replicate [10]. Therefore, finding an antiviral drug able to block the viral replication without affecting the host's physiological functions remains challenging. For this reason, siRNA therapeutics represent a promising candidate. By inducing the RNAi machinery, siRNAs can, in theory, specifically downregulate any given target mRNA, whether endogenously expressed or as a product of viral infections. siRNAs can be designed to be virus-specific and, by downregulating key factors of the viral replication cycle, can prevent the replication and spreading of the virus [11]. siRNA therapeutics could thus become a new ally in the fight against viral infections. After investigating the replication steps as well as the genomic regions of SARS-CoV-2 that can be targeted by siRNA, we identified an siRNA sequence targeting the highly conserved region open reading frame 1 (ORF1), which is part of the genomic RNA of the virus and which serves as a template for the translation of polyprotein 1ab (Pp1ab) [12]. Our previous study showed high efficacy of the newly developed siRNA in blocking the replication of SARS-CoV-2 as well as conservation of the target sequence in the current SARS-2 variants [12]. Two major advantages of an antiviral siRNA treatment could therefore be specificity for viral factors and therapeutic index. Considering that the lungs are the entry port for the virus and that represent the main site of infection and viral replication, pulmonary delivery is a desirable route of administration, particularly for antiviral siRNA [13]. Local siRNA administration to the lungs could represent an effective strategy against respiratory viral infections treatment due to the high surface area of the lungs and relatively low nuclease activity compared to systemic administration. Interestingly, a recent study by Azzi et al. reported that subjects who had received two doses of the COVID-19 vaccine and who presented high serum IgG antibody titers only had low saliva levels of neutralizing antibodies, indicating that local mucosal immunity at the virus entry site to the airways was not efficiently developed after vaccination. Therefore, pulmonary local administration could be beneficial to increase the immunity against viral infections [14]. Despite the advantages of the pulmonary route, lungs also present some hurdles that must be overcome for achieving the desired target site and down-regulation effect. Branching of the airways, mucociliary clearance and presence of mucus are the main factors hampering delivery of siRNA to target cells in the lungs [15]. Therefore, formulation of siRNA with a suitable delivery system is crucial for therapeutic siRNA activity.

Several nanocarriers have been developed in the last years for siRNA, mainly based on lipids, polymers or peptides [16]. Considering the pulmonary administration route, the encapsulation of siRNA in a polymer-based system appears preferable. While lipid-based systems might be affected by stability problems once nebulized for inhalation

[17], polymer-based formulations can be easily nebulized or processed to produce a dry powder for inhalation [18]. On this basis, we decided to formulate siRNA with VIPER (virus-inspired polymer for endosomal release), a block copolymer that showed high efficiency for both pDNA [19] and siRNA [20] delivery. In addition to protecting the cargo and enhancing cellular uptake, VIPER polymer also showed improved endosomal escape of siRNA, which is considered the bottleneck for non-viral RNA delivery systems [21]. The block copolymer is composed of a hydrophilic block, responsible for the encapsulation of the negatively charged siRNA by electrostatic interactions, and a hydrophobic, pH-sensitive block entrapping the lytic peptide melittin. Melittin is a peptide derived from bee venom with membrane-lytic activity. At acidic pH, the hydrophobic block undergoes a conformational change that leads to the exposure of the peptide, which can exert its lytic activity towards the endosome and consequently release the siRNA in the cytosol for initiating the RNAi machinery [19]. Previous studies suggested the suitability of VIPER polymer for the delivery of siRNA to the lungs [20]. Therefore, we further investigated this aspect to develop a formulation that can be efficiently delivered to lung epithelial cells, which are the main site of infection for SARS-CoV-2, for subsequent suppression of viral replication. To further explore the translatability of our findings, we established an air-liquid interface (ALI) culture of lung epithelial cells to understand the behavior of the polyplexes in a more sophisticated 3D culture model [22]. Furthermore, to close the gap between *in vitro* and *in vivo* correlation, we tested the activity of the VIPER polyplexes against wild type SARS-CoV-2 virus in human precision-cut lung slices (PCLS), which are living 3D tissue explants that retain the main features of the lung in terms of cellular diversity as well as anatomical structure [23]. Additionally, *in vivo* distribution and delivery to various cell types in the lung as well as toxicity and immunogenicity were investigated.

The aim of this study was the development of a pulmonary delivery system that can efficiently and selectively target lung epithelial cells and can efficiently block the replication of SARS-CoV-2. In this regard, VIPER polyplexes showed optimal parameters for pulmonary administration and high gene silencing efficiency *in vitro*. Additionally, the formulation was stable in presence of both lung surfactant and mucin, and penetrated the mucus layer secreted by Calu-3 cells cultured at the air-liquid interface. VIPER polyplex uptake in lung epithelial cells without toxic or immunogenic side effects was confirmed *in vivo* and their antiviral activity against SARS-CoV-2 was validated in the ALI culture model as well as *ex-vivo* human PCLS 3D lung model.

2. Experimental methods

2.1. Materials

Polyethylenimine 25 kDa was purchased from BASF (Ludwigshafen, Germany). RPMI-1640 medium, EMEM medium, DMEM-F12 medium, 0.05% and 0.25% trypsin-EDTA, heat-inactivated fetal bovine serum (FBS), penicillin/streptomycin (P/S), FluorSave, paraformaldehyde, alcian blue solution and Tween20 were purchased from Sigma-Aldrich (St. Louis, Missouri, USA). SYBR Gold dye, Lipofectamine 2000, Rhodamine Phalloidin, AF488-wheat germ agglutinin, (4',6-diamidino-2-phenylindole (DAPI), ZO-1 rabbit polyclonal antibody, AF488-anti-rabbit secondary antibody and Alexa Fluor™ 647 NHS Ester were obtained from Life Technologies (Carlsbad, California, USA). PneumaCult ALI differentiation medium, hydrocortisone and heparin were purchased from Stemcell Technologies (Vancouver, Canada). Transwell® polyester membrane cell culture inserts were purchased from Corning (New York, USA). Dicer substrate double-stranded siRNA (DsiRNA) targeting the enhanced green fluorescent protein gene, human GAPDH and scrambled non-specific DsiRNA as well as amine-modified siRNA were purchased from Integrated DNA Technologies (IDT, Coralville, Iowa, USA).

Table 1

Sequences of siRNAs used in the study. nt, nucleotides; O1–3, ORF1-specific siRNAs 1–3; Luc = Firefly Luciferase; A = Adenine; C = Cytosine; G = Guanine; U = Uracil; T = Thymine; Luc, Firefly Luciferase; *, Phosphorothioate linkage; [], 2'-O-Methyl modification; Fluoro, 2' Fluoro modification; A, Adenine; C, Cytosine; G, Guanine; U, Uracil.

Name	Sense strand (5'-3')	Antisense strand (5'-3')	Length (nt)	
			Sense	Antisense
O1	CCAAAUGUGCCUUUCAACUTT	AGUUGAAAGGCACAUUUGGUU	21	21
O3	GGUACUUGGUAGUUUAGCUTT	AGCUAAACUACCAAGUACCAU	21	21
siLuc	CGUACGCGGAAUACUUCGATT	UCGAAGUAUUCGCGUACGUG	21	21
O1*	[C]*-[C]*-[A]-[A]-[A]-[U]-FluoroG-[U]-FluoroG-FluoroC-FluoroC-[U]-[U]-[U]-[C]-[A]-[A]-[C]-[U]	[A]*-FluoroG*-[U]-[U]-[G]-FluoroA-[A]-FluoroA-FluoroG-[G]-[C]-[A]-[C]-FluoroA-[U]-FluoroU-[U]-[G]-[G]*-[U]*-[U]	19	21
O3*	[G]*-[G]*-[U]-[A]-[C]-[U]-FluoroU-[G]-FluoroG-FluoroU-FluoroA-[G]-[U]-[U]-[U]-[A]-[G]-[C]-[U]	[A]*-FluoroG*-[C]-[U]-[A]-FluoroA-[A]-FluoroC-FluoroU-[A]-[C]-[C]-[A]-FluoroA-[G]-[U]-[U]-[U]-[A]-[C]-[C]*-[A]*-[U]	19	21
siLuc*	[C]*-[G]*-[U]-[A]-[C]-[G]-FluoroC-[G]-FluoroG-FluoroA-FluoroA-[U]-[A]-[C]-[U]-[U]-[C]-[G]-[A]	[U]*-FluoroC*-[G]-[A]-[A]-FluoroG-[U]-FluoroA-FluoroU-[U]-[C]-[C]-[G]-FluoroC-[G]-FluoroU-[A]-[C]-[G]*-[U]*-[G]	19	21

2.1.1. Design of SARS-CoV-2 targeting siRNAs

The SARS-CoV-2 specific siRNAs were previously described [12] and target highly conserved regions within ORF1 of the SARS-CoV-2 genome. Chemically unmodified siRNAs were designed as symmetric 21-mers with 2 nucleotide overhangs at 3' ends of both strands with the sense strand overhang consisting of dTdT. An siRNA targeting Firefly Luciferase (siLuc) was designed as negative control. Chemically unmodified siRNAs were purchased in desalted form (Microsynth AG, Balgach, Switzerland), resuspended and maintained in RNase free water upon arrival. Chemically modified versions of ORF1-targeting siRNAs and siLuc were designed in an asymmetric fashion using a previously described design and chemical modification pattern [12]. In brief, all nucleotides of the siRNA were subjected to a 2'-O-Methyl modification (2'OMe) except nucleotides at positions 7, and 9–11 of the siRNA sense-, as well as positions 2, 6, 8, 9, 14, and 16 of the antisense-strand (all 5'-3' direction), which contained 2'-Fluoro modifications (2'F) instead. Additionally, two consecutive nucleotides at both ends of the siRNA antisense strand, as well as at the 5' end of the sense strand were incorporated with phosphorothioate linkages (for details see Table 1). Chemically modified siRNAs were synthesized by Eurogentec (Liège, Belgium) at a 40 nmol scale and purified by High Performance Liquid Chromatography (HPLC). The siRNAs were obtained in desalted form and reconstituted in RNase free water at a concentration of 20 mM.

2.2. VIPER synthesis

The block co-polymer p(OEGMA300_{8,6}-co-DMAEMA₅₀)-b-p(DIPAMA_{25,3}-co-PDSEMA₁) was synthesized via reversible addition-fragmentation chain transfer (RAFT) polymerization as described previously. The cysteine-terminated melittin peptide (cys-melittin) was conjugated to the PDSEMA side chain by disulfide exchange, purified and characterized as previously reported [19,24].

2.3. Preparation of siRNA polyplexes

Polymer/siRNA polyplexes were prepared by first dissolving polyethylenimine 25 kDa and VIPER polymer separately in RNase free water at a concentration of 1 mg/ml, and then sterilizing the solution through a 0.22 µm filter. Stocks of polymer and siRNA were further diluted in a sterile 5% glucose solution to reach the desired concentration. An equal volume of each polymer was added to a defined amount of siRNA solution and incubated for 20 min to yield polyplexes at a defined N/P ratio (N/P 6 for PEI 25 kDa, N/P 10 for VIPER, if not stated otherwise). All calculations were based on previous studies with pDNA as well as siRNA [19,20].

2.4. Hydrodynamic diameter and zeta (ζ) potential measurements of siRNA polyplexes

Hydrodynamic diameters and polydispersity indices were measured by dynamic light scattering (DLS using a Zetasizer Nano ZS (Malvern Instruments Inc., Malvern, UK). Polyplexes were prepared with scrambled siRNA in 5% glucose solution, added to a disposable micro-cuvette and measurements were performed at 173° backscatter angle running 10 runs three times per samples. Results are presented as average size (nm) ± SD. The samples were further diluted to 700 µl with 5% glucose and transferred to a folded capillary cell for ζ-potential measurements, which were analyzed by Laser Doppler Anemometry (LDA). Samples were read in triplicates, with each run consisting of 30–50 scans. Results are presented in mV ± SD.

2.5. Polyplex stability in presence of mucin or lung surfactant

To test the stability of polyplexes in an environment that mimic the lung environment, a modified SYBRgold assay in presence of lung surfactant Alveofact or mucin was performed as previously reported [25]. PEI and VIPER polyplexes were prepared with 30 pmol siRNA in 100 µl 5% glucose. Once polyplexes were formed, 50 µl of a serial dilution of Alveofact or mucin were added (final concentration: 0, 0.0005, 0.005, 0.05, 0.25, 0.5 mg/ml) and incubated for 20 min. Afterwards, samples were distributed in a black 96-well-plate, and 30 µl of 4× SYBRgold solution were added to each well and incubated for 10 min in the dark. Fluorescence was then measured on a plate reader (Tecan, Männedorf, Switzerland) at excitation wavelength of 485/20 nm and emission wavelength of 520/20 nm. To account for autofluorescence of mucin, free siRNA samples were prepared in the presence of the corresponding concentration of mucin. Fluorescence of free siRNA represents 100% siRNA release. All measurements were performed in triplicates, and results are presented as mean values ± SD.

2.6. In vitro characterization of siRNA/VIPER polyplexes in a lung epithelial cell line

2.6.1. Cell culture

The human non-small cell lung carcinoma cell line stably expressing the reporter gene EGFP (H1299/GFP) was cultured in RPMI-1640 medium supplemented with 10% FBS, 1% P/S and 0.4% G418. Cells were passaged every 3 days with trypsin 0.05% and subcultured in 75 cm² flasks. Cells were maintained in a humidified atmosphere at 37 °C and 5% CO₂.

2.6.2. In vitro GFP protein downregulation

To determine the ability of polyplexes to efficiently downregulate protein expression, H1299/GFP cells were used. H1299/GFP cells were seeded in a 24-well-plate at a density of 25.000 cells/well in 500 µl of

medium and incubated at 37 °C and 5% CO₂. The day after, cells were transfected with 100 µl of VIPER or PEI polyplexes containing 100 pmol of GFP or scrambled siRNA sequence. Lipofectamine lipoplexes were used as positive control. Cells were incubated for 48 h at 37 °C and 5% CO₂. Once the incubation time was completed, cells were trypsinized, washed two times in PBS and PBS/2 mM EDTA respectively and analyzed via flow cytometry (Attune NxT, Thermo Fischer Scientific, Waltham, Massachusetts, USA) for the median fluorescence intensity (MFI) of GFP protein expression using 488 nm excitation and a 530/30 nm bandpass emission filter. Samples were measured in triplicates, with each sample gated by morphology based on forward/sideward scattering for a minimum of 10.000 viable cells. Results are displayed as mean values ± SD.

2.6.3. *In vitro* GAPDH gene knockdown

For gene silencing experiments, 24 h prior to transfection 100.000 H1299/GFP cells were seeded in a 12-well-plate and incubated at 37 °C and 5% CO₂. Cells were transfected with 100 µl of VIPER or PEI polyplexes containing 100 pmol of GAPDH or scrambled siRNA. Positive controls consisted of Lipofectamine 2000 lipoplexes while negative controls consisted of blank/untreated cells. After 24 h, cells were harvested and processed to isolate total RNA using the PureLink RNA mini kit according to the manufacturer's protocol (Life Technologies, Carlsbad, California, USA). cDNA was synthesized from total RNA using the high-capacity cDNA synthesis kit (Applied Biosystems, Waltham, Massachusetts, USA). Afterwards, the obtained cDNA was diluted 1:10 and a qPCR performed using the SYBR™ Green PCR Master Mix (Thermo Fisher Scientific) with primers for human GAPDH (Qiagen, Hilden Germany) and β-actin (Qiagen, Hilden, Germany) for normalization. Cycle thresholds were acquired by auto setting within the qPCRsoft software (Analytic Jena AG, Jena, Germany). Values are given as mean values ± SEM.

2.6.4. *In vitro* cytotoxicity in lung cells

2.6.4.1. Cell viability. Cell viability was assessed using the MTT assay. H1299/GFP cells were seeded at a density of 10.000 cells/well in 100 µl medium in a 96-well-plate 24 h prior to transfection. Cells were transfected with PEI and VIPER polyplexes containing 20 pmol scrambled siRNA at different N/P ratios (6, 10 and 15 respectively) and incubated for 24 h at 37 °C and 5% CO₂. Once the incubation time was completed, medium was removed and 100 µl of a sterile 0.5 mg/ml 3-(4,5-dimethylthiazol-2-yl)-2,5-diphenyltetrazolium bromide (MTT) solution was added to the cells and incubated for 3 h at 37 °C and 5% CO₂. Medium was then removed, and 200 µl of DMSO was added to each well to dissolve formazan crystals. Absorbance was then read at 570 nm using a microplate reader (Tecan, Männedorf, Switzerland). Results are given as mean of values of triplicates ± SD.

2.6.4.2. LDH release. The effect of polyplexes on membrane integrity was assessed by measuring the release of lactate dehydrogenase (LDH) in the extracellular medium using the CytoTox96® Non-Radioactive Cytotoxicity Assay kit (Promega, Madison, Wisconsin, USA) according to the manufacturer's protocol. Briefly, 5.000 H1299/cells were seeded in a 96-well-plate in 100 µl medium 24 h prior to transfection. Cells were treated with PEI and VIPER polyplexes containing 20 pmol siRNA at different N/P ratios (6, 10 and 15 respectively) and incubated for another 24 h. Afterwards, 50 µl of supernatant was transferred to a fresh 96-well-plate and 50 µl of substrate mix was added and incubated for 30 min at room temperature protected from light. Subsequently, 50 µl of stop solution was added and absorbance was measured at 490 nm using a microplate reader (Tecan, Männedorf, Switzerland). Untreated cells were used as negative control, while cells treated with lysis buffer represented 100% LDH release. Results are given as mean values of triplicates ± SD.

2.7. Polyplex behavior in mucus-secreting Calu-3 cells grown at the air-liquid interface

2.7.1. Cell culture

Calu-3 cells were obtained from LGC Standards GmbH (Wesel, Germany). Cells were maintained in EMEM medium supplemented with 10% FBS and 1% P/S. Cells were passaged once 80% confluence was reached and subcultured in 75 cm² flasks. Cells were maintained in a humidified atmosphere at 37 °C and 5% CO₂.

Calu-3 cells were seeded at a density of 250.000 cells onto uncoated Transwell® polyester cell culture inserts (6.5 mm, 0.4 µm pore size) in 100 µl medium, while 700 µl medium were added to the basolateral chamber. After 72 h, the apical medium was removed to obtain air-liquid interface conditions, while the medium from the basolateral chamber was replaced with 200 µl of PneumaCult™ ALI medium (STEMcell technology, Vancouver, Canada) and replaced every two days. Experiments were performed once TEER values ≥300 Ω*cm² were reached and a stable polarized epithelial layer was formed, as measured with an EVOM epithelial volt/Ω meter (World Precision Instruments, Sarasota, USA).

To confirm the secretion of mucus by Calu-3 cells grown under ALI conditions, an alcian blue staining was performed. Briefly, cells were incubated for 15 min with 100 µl alcian blue solution and washed 3 times with 200 µl PBS. Cells were then mounted on glass slides using FluorSave (Merck Millipore, Darmstadt, Germany) reagent and analyzed using a BZ-8100 (Biozero) fluorescence microscope (Keyence, Osaka, Japan). Images were processed with Fiji distribution of ImageJ.

To verify the expression of tight junctions when cells were cultured at ALI, the expression of zonula occludens protein-1 (ZO-1) was evaluated. Briefly, 7 days after air-lift, cells were fixed in 4% PFA for 15 min, blocked for 1 h in 5% BSA blocking buffer and then incubated overnight with a 1:100 dilution of ZO-1 rabbit polyclonal antibody (Life Technologies, Carlsbad, California, USA). Afterwards, cells were incubated for 1 h with a 1:200 dilution of AF488-anti-rabbit secondary antibody (Life Technologies, Carlsbad, California, USA). Once the incubation time was completed, cells were washed two times with PBS, and nuclei were stained with a 0.5 µg/ml solution of 4',6-diamidino-2-phenylindole (DAPI) for 15 min. Finally, cells were washed two times with PBS and mounted on glass slides with FluorSave reagent. Samples were analyzed with a SP8 inverted confocal scanning microscope (Leica Camera, Wetzlar, Germany). The images were exported and processed with the Leica Image Analysis Suite software.

2.7.2. Cell uptake study

For microscopy experiments, amine-modified siRNA was labeled with succinimidyl ester (NHS) modified AlexaFluor647 fluorescent dye according to the manufacturer's protocol and purified via ethanol purification to obtain AF647-siRNA as previously reported [26].

To evaluate the delivery of polyplexes to Calu-3 monolayers, cells were transfected with PEI and VIPER polyplexes containing 100 pmol AF647-siRNA for 24 h. Once the incubation time was completed, monolayers were fixed in 4% PFA for 15 min, washed 3 times with PBS and permeabilized with PBS + 0.3% Tween20 for 10 min. Cells were then incubated with rhodamine phalloidin for 60 min. Nuclei were stained with a 0.5 µg/ml solution of 4',6-diamidino-2-phenylindole (DAPI) for 15 min. Finally, cells were washed two times with PBS, mounted on glass slides using FluorSave reagent and analyzed with a SP8 inverted confocal laser scanning microscope (Leica Camera, Wetzlar, Germany). The images were exported from the Leica Image Analysis Suite and processed with the Fiji distribution of ImageJ.

2.7.3. Mucus penetration study

The ability to overcome the mucus barrier was assessed by transfecting Calu-3 monolayers with PEI and VIPER polyplexes containing 100 pmol AF647-siRNA for 24 h. Afterwards, cells were incubated for 15 min with AF488-wheat germ agglutinin at 37 °C and 5% CO₂ to stain

the mucus layer. Cells were then washed two times with PBS and mounted on glass slides using FluorSave reagent and immediately analyzed with a SP8 inverted confocal laser scanning microscope (Leica Camera, Wetzlar, Germany). The images were exported from the Leica Image Analysis Suite and processed with the Fiji distribution of Image J.

2.7.4. GAPDH knockdown in Calu-3 cells at ALI

In order to measure the transfection efficiency of polyplexes in a more sophisticated *in vitro* model, Calu-3 monolayers were transfected with PEI and VIPER polyplexes containing 100 pmol GAPDH or scrambled siRNA for 24 h at 37 °C and 5% CO₂. Positive controls consisted of Lipofectamine 2000 lipoplexes while negative controls consisted of blank/untreated cells. Cells were then detached, and RNA was extracted using the PureLink RNA mini kit according to the manufacturer's protocol. Samples were further processed for cDNA synthesis and qPCR as described above. Values are given as mean of triplicates ± SEM.

2.7.5. Immunofluorescence staining and confocal imaging of ACE-2 receptor on Calu-3 cells

To evaluate the ACE-2 receptor expression on Calu-3 cells, the membranes were cut out of the transwells in circles and embedded on the basolateral side with Cryomatrix embedding medium (Shandon Cryomatrix, Thermo Fisher Scientific, Waltham MA, USA) on dry ice. Calu-3 cells were then covered on the apical side with Cryomatrix. Embedded cells were frozen on dry ice and stored at –80 °C for further processing. Later, the embedded cells were cut into cryosections (7 µm) using a Kryostat CM3050S (Leica Biosystems, Nussloch, Germany). Cryosections were dried for 4 h on SuperFrost plus glass slides (Menzel-Glaeser, Germany) and were then fixed with ice cold methanol and acetone (1:1) for 10 min. Glass slides were washed three times for 5 min with cold 1× Wash Buffer (WB) (medac diagnostika, Wedel, Germany) with shaking. Unspecific binding sites were blocked with 10% BSA for 20 min. Slides were then incubated with a primary antibody against human ACE-2 receptor ((AF933), R&D systems, Minneapolis, MN, USA) at a concentration of 5 × 10³ µg/ml in 1× WB, containing 1% BSA for 1 h. Cells were washed three times for 5 min with cold WB before slides were treated with a 1:500 dilution of a donkey anti goat IgG H&L Alexa Fluor® 647 preadsorbed (ab150135, Abcam, Cambridge, MA, USA) antibody in WB/BSA for 30 min in the dark. Slides were counterstained and embedded with ProLong Gold Antifade Moutant with DAPI (4',6'-diamidino-2-phenylindole) (Life Technologies, Thermo Fisher Scientific, Waltham MA, USA) solution overnight in the dark. For control sections, only the secondary antibody was used. Fluorescence imaging was performed using a laser scanning confocal microscope LSM700 (Carl Zeiss, Wetzlar, Germany) with the Axio Imager 2 and the Software ZEN 2.3 lite (Carl Zeiss, Wetzlar, Germany). Images were taken with a Zeiss 63× oil immersion objective. The pictures were analyzed and modified regarding contrast and intensity, using ZEN 2.3 lite (blue edition). Nucleus staining (DAPI) was illustrated with the emission color blue, while Alexa Fluor 647 was shown in magenta. Scale bars were added using the free software ImageJ.

2.8. siRNA/VIPER polyplex activity against SARS-CoV-2 at the air-liquid interface

To test the activity of siRNA/VIPER polyplexes against wild-type SARS-CoV-2 virus, Calu-3 monolayers were transfected with 100 pmol of VIPER polyplexes containing 100 pmol ORF1#3 or luciferase siRNA as negative control 6 h before infection with 0.1 MOI wildtype SARS-CoV-2. After 24 h, RNA was extracted as described under 2.10.

Table 2

Oligonucleotides and cycling conditions used for polymerase chain reaction. A = Adenine; C = Cytosine; G = Guanine; T = Thymine; Rev. = reverse; s = second; RDRP = RNA-dependent RNA polymerase.

PCR name	Primer/probe sequences (5'-3') and cycling conditions
Beta-actin	Fw: CCACGAACTACCTTCAACTCCAT Rev.: TGTGTGGCGTACAGGTCTTTG
N	Fw: GACCCCAAATCAGCGAAAT Rev.: TCTGGTTACTGCCAGTTGAATCTG
RDRP	Fw: CGTCTGCGGTATGTGGAAAG Rev.: TAAGACGGGCTGCACTTACA
	Cycling conditions
	95 °C - 5 min
	45 Cycles: 95 °C - 15 s
	55 °C - 10 s
	72 °C - 25 s

2.9. Ex vivo activity of siRNA/VIPER polyplexes in human precision-cut lung slices

2.9.1. Human tissue, ethics statement and human precision-cut lung slices (hPCLS)

Human tissue was obtained from the CPC-M bioArchive at the Comprehensive Pneumology Center (CPC), from the University Hospital Großhadern of the Ludwig-Maximilian University (Munich, Germany) and from the Asklepios Biobank of Lung Diseases (Gauting Germany). Participants provided written informed consent to participate in this study, in accordance with approval by the local ethics committee of the Ludwig Maximilian University Munich, Germany (Project 19–630). Precision-cut lung slices (PCLS) were prepared as described before [27,28]. Briefly, PCLS were prepared from tumor-free peri-tumor tissue. The lung tissue was inflated with 3% agarose solution and solidified at 4 °C. afterwards, 500 µm thick slices were cut from tissue blocks using a vibration microtome (HyraXV50) (Karl Zeiss AG, Oberkochen, Germany). PCLS were cultured in DMEM F-12 medium supplemented with 0.1% FBS. Prior to experiments, PCLS cut by means of a biopsy puncher into 4 mm in diameter PCLS punches.

2.9.2. Establishment of wild-type SARS-CoV-2 infection in hPCLS

PCLS samples were prepared as described above and cultured with Dulbecco's Modified Eagle Medium (DMEM) F-12 supplemented with L-Glutamine, HEPES, 10,000 IE Penicillin, 10,000 IE Streptomycin and 0.1% fetal bovine serum. For each sample, three PCLS were placed in a 48 well plate in 500 µl medium and infected with 300,000 (pure), 30,000 (0.1×) or 3,000 (0.01×) plaque-forming units (PFU) SARS-CoV-2. PCLS were washed with PBS after 1 h and RNA extracted as described under 2.10 after 24, 48 and 72 h.

2.9.3. Polyplex activity against wild-type SARS-CoV-2 in hPCLS

PCLS samples were prepared as described above and cultured with Dulbecco's Modified Eagle Medium (DMEM) F-12 supplemented with L-Glutamine, HEPES, 10,000 IE Penicillin, 10,000 IE Streptomycin and 0.1% fetal bovine serum. For each sample, three PCLS were placed in a 48 well plate in 500 µl medium and transfected with VIPER polyplexes containing 60 pmol siRNA against ORF1 as well as non-targeting siRNA six hours before being infected with wildtype SARS-CoV-2. For infection, 300,000 plaque-forming units (PFU) SARS-CoV-2 were added to each well, which contained PCLS with an estimated cell number of 300,000 cells, resulting in an approximated MOI of 1.0. After 24 h, RNA was extracted as described under 2.10.

2.10. Nucleic acid extraction and qPCR

Nucleic acid was extracted from ALI cultures using the NucleoSpin RNA kit (Macherey-Nagel; Düren, Germany). To isolate RNA from PCLS, samples were first homogenized using the TissueLyzer LT (Qiagen, Order # 85600) and then RNA was isolated using TRIzol

Table 3

PEI and VIPER polyplexes hydrodynamic diameter, polydispersity index and zeta potential.

Formulation	Size (nm \pm SD)	PDI (\pm SD)	ζ potential (mV \pm SD)
siRNA PEI	85.5 \pm 6.8	0.25 \pm 0.01	12.4 \pm 6.2
siRNA VIPER	55.8 \pm 9.5	0.39 \pm 0.03	9.5 \pm 2.4

(ThermoFischer Scientific) according to instructions. cDNA was synthesized with the Superscript™ III First-Strand Synthesis System (Thermo Fisher Scientific; Dreieich, Germany). SARS-CoV-2 RNA was quantified by qPCR performed on a LightCycler® 480 (Roche Holding AG; Basel, Switzerland) using primers specific for the N region (total viral RNA) or the RNA dependent RNA polymerase (Rdrp) region (as measure of genomic viral RNA [gRNA]) of SARS-CoV-2 and beta-actin as a house-keeping gene. For primer sequences and cycling conditions, see Table 2.

2.11. *In vivo* polyplex distribution in the lung and pro-inflammatory effects following pulmonary delivery

All animal experiments were approved by a Wayne State University Institutional Animal Care and Use Committee (IACUC). Female BALB/c mice were purchased from Charles Rivers Laboratories (Wilmington, Massachusetts, USA) and used at 5 weeks of age. Mice were intratracheally instilled (under ketamine/xylazine anaesthesia) with PEI and VIPER polyplexes containing 2 nmol AF647-siRNA. Control groups were administered with 5% glucose only. After 48 h, mice were sacrificed under i.p. ketamine/xylazine anaesthesia, exsanguinated and perfused with PBS. BALF and lung cell suspensions were prepared as reported before [29]. Serum was obtained from clotted blood. Lung cell suspensions were counterstained with BB515 labeled rat anti-mouse CD45 (30-F11, 1:40, BD Biosciences), pacific orange labeled F4/80 (1:100, Invitrogen), BV421 labeled anti-tubulin β 3 (1:100, Biolegend), anti-prosurfactant protein C (1:100, Abcam), mouse anti-rabbit PE-Cy7 (1:200, Santa Cruz Biotechnology), anti-uteroglobin antibody (1:100, Abcam) and mouse anti-rabbit AF594 (1:200, Invitrogen) following the manufacturer's protocol. The analysis was performed on a BDLSR Fortessa flow cytometer. The different populations of leukocytes (CD45+), macrophage/monocytes (F4/80+), Type II pneumocytes (proSPC+), ciliated cells (tubulin beta +) and club cells (CD31 +) were gated, and the MFI of siRNA-AF647 in the different cell populations was quantified. The concentration of proinflammatory cytokines in BALF and serum was determined using the mouse LEGENDplex ELISA kit (BioLegend, San Diego, California). Values are given as mean \pm SEM with $n = 4$.

2.12. Statistics

Statistical analysis was performed with GraphPad Prism 5 software using One-Way or Two-Way ANOVA with Turkey post-hoc test, with $p > 0.05$ considered not significant (ns) and $*p < 0.05$, $**p < 0.01$, $***p < 0.005$ considered significantly different.

3. Results and discussion

3.1. Characterization of polyplexes

Size and surface charge are among the most important parameters that need to be considered when designing an efficient drug delivery system. The parameters should be optimized for the intended route of administration and tuned towards the right size and zeta potential. Considering that the lungs are the organs mainly affected by SARS-CoV-2 infection, we aimed at achieving a formulation optimized for pulmonary administration. In previous work, we identified N/P 6 and 10 as optimal for pulmonary PEI and VIPER polyplex delivery, respectively, and have thus used these formulations throughout this study [20,30]. siRNA/PEI and siRNA/VIPER polyplexes were analyzed via dynamic light scattering for size and polydispersity index, and by Lased Doppler Anemometry for zeta potential. Both PEI and VIPER polyplexes showed desirable hydrodynamic diameters for pulmonary delivery of 85.52 nm and 55.78 nm (intensity-weighted) respectively (Table 3). Nanoparticles formed with VIPER polymer, however, showed smaller sizes, which could help avoid clearance by macrophages and enhance diffusion through the mucus mesh [31]. In terms of PDI, PEI and VIPER polyplexes showed values of 0.25 and 0.39 respectively. The higher PDI values observed for VIPER are possibly linked to the presence of the peptide melittin in the structure of the polymer, which could lead to an increase in PDI. Nonetheless, PDI could be reduced by introducing a microfluidic approach in future development [32,33]. Similar zeta potential values were observed for PEI and VIPER polyplexes. Both formulations presented a positive zeta potential of about 10 mV in line with expectations, due to the cationic nature of the polymers being tested.

3.2. Stability of polyplexes in presence of mucin and lung surfactant

When treating lung diseases, pulmonary delivery is the preferred route of administration due to the large surface area of the lungs, absence of serum proteins and limitation of systemic side effects [34]. Especially in the case of respiratory viral infections, such as in the recent pandemic caused by SARS-CoV-2, pulmonary administration ensures that the payload will directly reach the site of infection, the lung

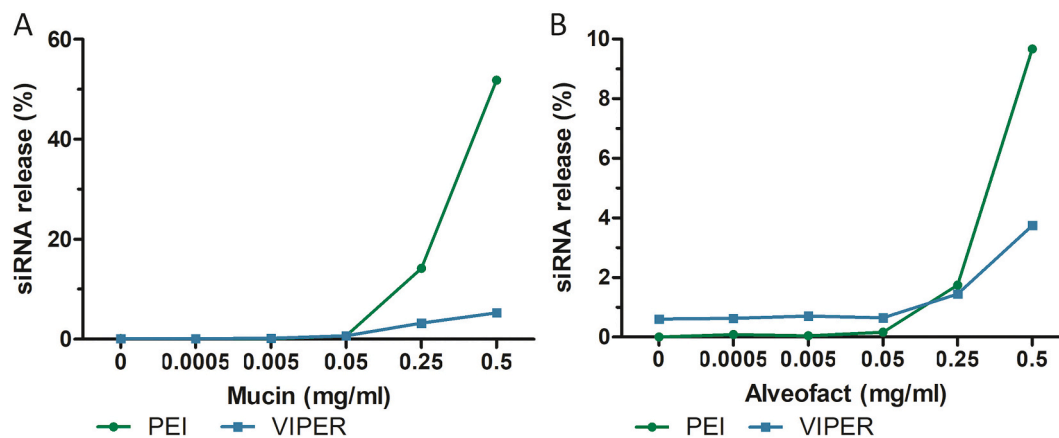


Fig. 1. Stability of polyplexes at increasing concentration of (A) mucin and (B) lung surfactant was tested by modified SYBR gold assay after 20 min incubation. Free siRNA represents 100% siRNA release. (Mean \pm SD, n03). Green square: siRNA release from PEI polyplexes. Blue circle: siRNA release from VIPER polyplexes. (For interpretation of the references to color in this figure legend, the reader is referred to the web version of this article.)

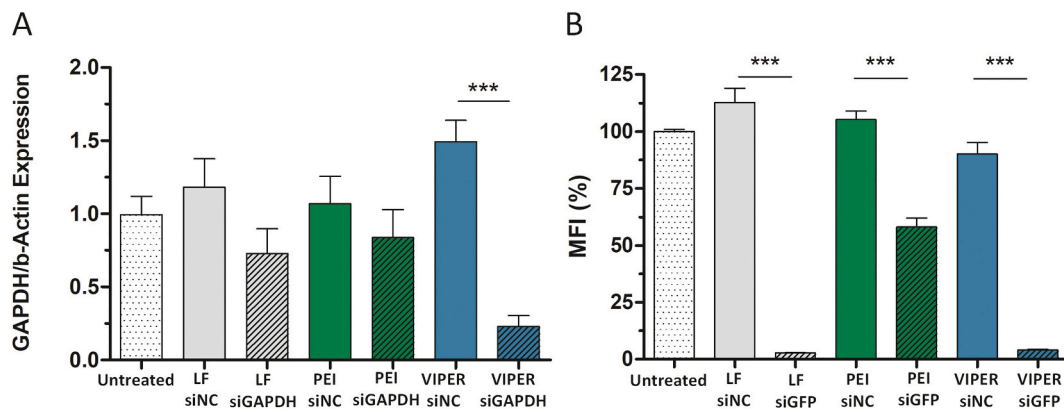


Fig. 2. *In vitro* downregulation activity of PEI and VIPER polyplexes in a H1299 cell line stably expressing EGFP. (A) GAPDH gene knockdown efficiency of PEI and VIPER polyplexes 24 h after transfection with polyplexes. Blank samples consisted of H1299GFP cells treated with 5% glucose only. Negative controls consisted of polyplexes encapsulating scrambled siRNA. Positive controls consisted of Lipofectamine2000 lipoplexes with 100 pmol siGAPDH. GAPDH expression was normalized with β -actin expression and quantified by qRT-PCR. Data points indicate mean \pm SEM. (B) GFP knockdown was measured by flow cytometry 48 h after transfection with PEI and VIPER polyplexes with 100 pmol siGFP. Blank samples consisted of H1299GFP cells treated with 5% glucose only. Negative controls consisted of samples treated with polyplexes encapsulating scrambled siRNA. Positive controls consisted of Lipofectamine2000 (LF) lipoplexes with 100 pmol siGFP. Data points indicated mean \pm SD ($n = 3$). One-Way ANOVA, *** $p < 0.005$.

epithelium, avoiding problems related to systemic administration. Nonetheless, biological barriers should be carefully addressed when considering pulmonary delivery. The lung epithelium is covered by a mucus layer that hampers the delivery of the cargo to the underlying cell layer. The negatively charged mucin glycoproteins represent the main component of the lung mucus layer and they are thought to be responsible for instability of polyplexes in mucus [35]. Additionally, deeper lungs are covered by lung surfactant, which contains high concentration of phospholipids. Therefore, we tested the stability of VIPER and PEI polyplexes in the presence of increasing concentrations of mucin and Alveofact®, a commercially available lung surfactant, by a modified SYBR gold assay [25]. As it can be observed in Fig. 1, VIPER showed increased stability at increasing concentrations of mucin in comparison to PEI. At a concentration of mucin as high as 0.5 mg/ml, VIPER showed only negligible release of siRNA, while PEI polyplexes released about 60% of their load. Both polymers showed better stability in lung surfactant compared to mucin, but VIPER outperformed PEI, with a release of 4 vs. 10% of the siRNA load. A possible explanation for the increased stability of VIPER polyplexes in mucus and surfactant could be the presence of the hydrophilic OEGMA-co-DMAEMA block [36].

3.3. *In vitro* transfection efficacy in lung epithelial cells

The gene silencing activity of PEI and VIPER polyplexes was tested at the mRNA and protein level in a human non-small lung carcinoma cell line stably expressing GFP (H1299/GFP cells). PEI and VIPER polyplexes were prepared with 100 pmol siRNA at N/P 6 and N/P 10 respectively. To test the activity at the mRNA level, PEI and VIPER polyplexes were prepared with siRNA specific for the human GAPDH, an endogenously expressed housekeeping gene, as well as with scrambled siRNA as negative control. Positive controls consisted of lipofectamine/siGAPDH lipoplexes. The expression of GAPDH was measured via quantitative real time PCR and normalized to β -actin expression. The experiment showed that both PEI and VIPER polyplexes mediated a gene knockdown at the mRNA level, but VIPER showed the more robust activity, reaching about 80% gene silencing (Fig. 2B). A similar trend was also observed at the protein level, where the activity of the polyplexes was evaluated by quantifying the median fluorescence intensity (MFI) of the different samples and normalized for the untreated samples (100%). Also in this case, VIPER polyplexes achieved high gene silencing activities of about 90%, similarly to the one showed by the positive control lipofectamine. PEI polyplexes instead only suppressed about 40% of the GFP expression (Fig. 2A). This difference in activity is probably linked to the presence of

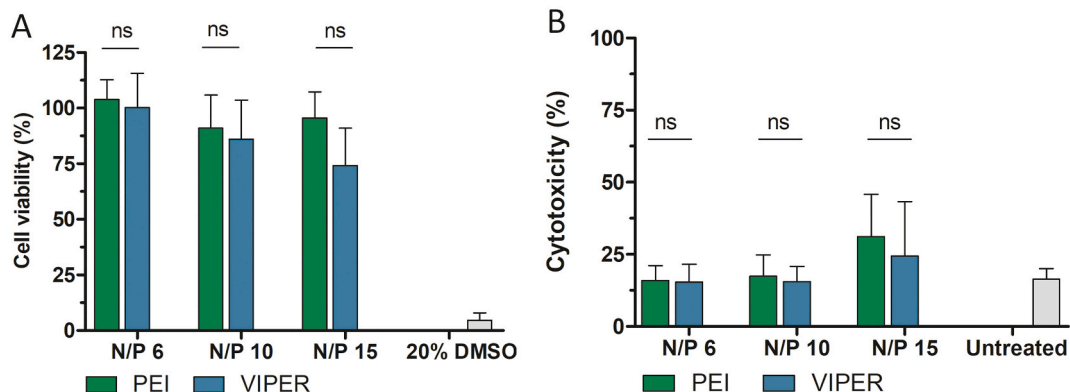


Fig. 3. Evaluation of cytotoxicity following incubation with PEI and VIPER polyplexes. (A) Evaluation of cellular viability by MTT assay of H1299/GFP cells incubated with PEI and VIPER with different N/P ratios: 6, 10 and 15. Positive controls consisted of cells treated with 20% DMSO. Data points indicate mean \pm SD ($n = 3$). One-Way ANOVA, ns = not significant. (B) Assessment of membrane integrity by measuring lactate dehydrogenase release of cells incubate with PEI and VIPER polyplexes at different N/P ratios: 6, 10, 15. Cells treated with lysis buffer correspond to 100% LDH release. Data points indicate mean \pm SD ($n = 3$). One-Way ANOVA, ns = not significant.

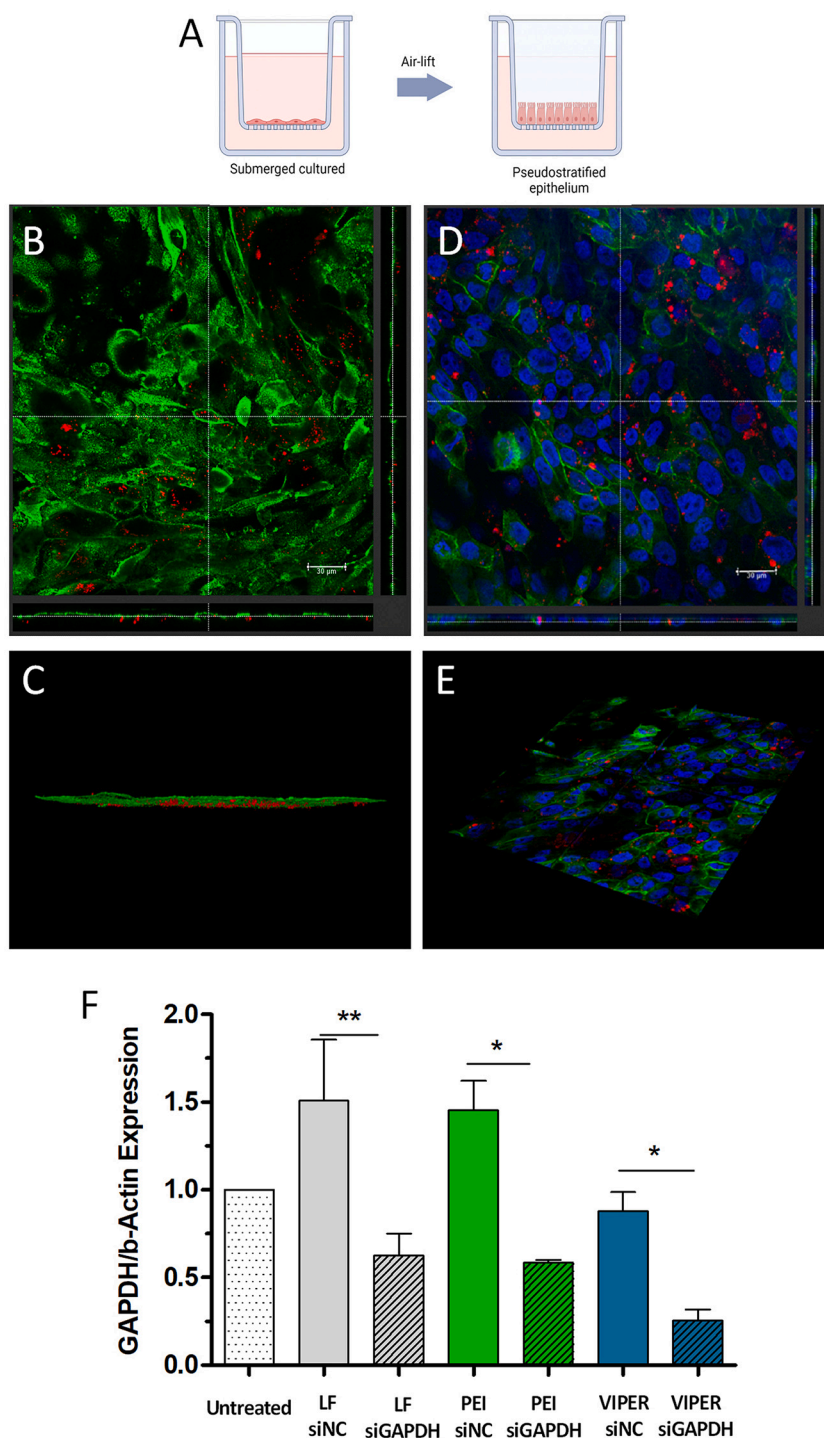


Fig. 4. Evaluation of AF647-siRNA/VIPER polyplexes delivery to Calu-3 cells grown at the air-liquid interface. (A) Schematic of the air-liquid interface culture model. Figure created with BioRender.com (B,C) Mucus penetration of AF647-siRNA/VIPER polyplexes in Calu-3 monolayers 24 h after transfection. (B) XY and XZ viewing direction. (C) 3D reconstruction. Red color represents AF647-siRNA, green color to the mucus layer stained with AF488-labeled wheat germ agglutinin. (D,E) Cell uptake of AF647-siRNA/VIPER polyplexes 24 h after transfection analyzed by confocal light scanning microscopy. (D) XY and XZ viewing direction. (E) 3D reconstruction. Red color corresponds to AF647-siRNA, green color to actin stained with rhodamine phalloidin and blue color corresponds to nuclei stained with DAPI. (F) GAPDH gene knockdown efficiency PEI and VIPER polyplexes in Calu-3 monolayers grown under ALI conditions 24 h after transfection with siGAPDH and scrambled siRNA as negative control. Blank samples consisted of Calu-3 monolayers treated with 5% glucose only. Positive controls consisted of Lipofectamine2000 lipoplexes with siGAPDH. GAPDH expression was normalized with β -actin expression and quantified via qRT-PCR. Data points indicate mean \pm SEM ($n = 3$). One-Way ANOVA, * $p < 0.05$, ** $p < 0.01$. (For interpretation of the references to color in this figure legend, the reader is referred to the web version of this article.)

melittin in the structure of VIPER, which is an endosomolytic peptide that has been studied for improving the activity of siRNA delivery agents [37]. By disrupting the endosomal membrane, melittin helps to release the siRNA in the cytosol and consequently improves the RNAi activity of the siRNA formulation [38].

3.4. *In vitro* cytotoxicity in lung epithelial cells

To test the compatibility of the formulations with living cells, PEI and VIPER polyplexes were incubated with H1299/GFP cells at different N/P ratios. The viability of the cells was measured via the MTT assay, a colorimetric assay used to measure the metabolic activity of the cells as

an indicator of cell viability. The experiment showed that both PEI and VIPER present an overall safe profile, with no reduction in cell viability in comparison to the untreated control for N/P 6 and 10, and a reduction by about 20% for VIPER at the highest N/P ratio tested of 15. The difference in cell viability for the two different polymers was not significant for any of the N/P ratios tested (Fig. 3A).

To further investigate the effect of the formulation on cell membrane integrity, an LDH assay was performed at the same conditions as the MTT assay. By measuring the release of lactate dehydrogenase enzyme in the supernatant, the assay gives a measure of the impact of the formulation on the membrane integrity. The cytotoxicity was measured by comparing the results to a 100% LDH release considered as maximal

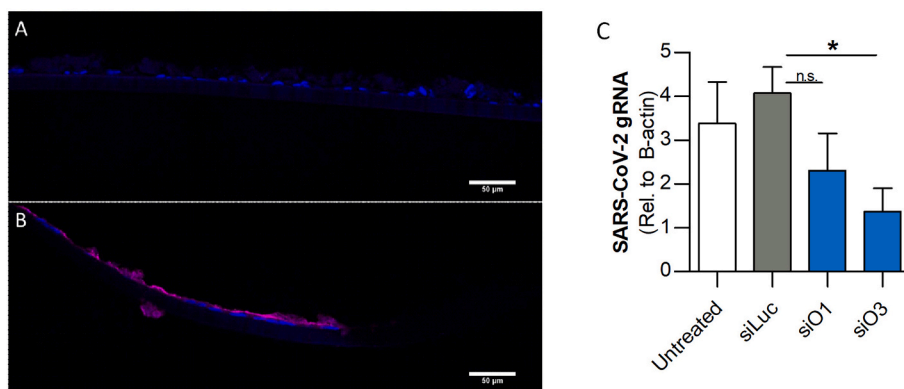


Fig. 5. Evaluation of siORF/VIPER polyplexes activity against wild-type SARS-CoV-2 infection in Calu-3 cells grown at the air-liquid interface. (A, B) The expression of ACE-2 receptor on the apical side of Calu-3 cells was confirmed by preparing sections of Calu-3 monolayers. Pink color represents AF944 staining of ACE-2 receptor, blue color represents nuclei staining with DAPI. (C) SARS-CoV-2 downregulation in Calu-3 monolayers after treatment with SARS-CoV-2 specific siRNAs O1 and O3/VIPER polyplexes and siLuc/VIPER polyplexes as negative control. Calu-3 cells were infected with wild type SARS-CoV-2 (MOI 0.1) 6 h after transfection with polyplexes. Data points indicate mean \pm SEM ($n = 3$). Statistical significance was calculated using One-way Anova with Dunnett's multiple comparisons correction. (For interpretation of the references to color in this figure legend, the reader is referred to the web version of this article.)

cytotoxicity as well as to untreated cells as negative control. PEI and VIPER showed a similar trend, with only negligible LDH release detected for N/P 6 and 10 with values similar to the ones observed for untreated cells, while higher release was observed for the highest N/P ratio tested. PEI and VIPER showed a similar trend in terms of LDH release, confirming that the presence of melittin in the formulation did not result in higher membrane damage nor increased toxicity (Fig. 3B). These results are in line with previously reported hemolysis data for plasmid/VIPER polyplexes and were explained by their pH-responsive behavior [19].

3.5. siRNA/VIPER polyplex delivery in an air-liquid interface culture system

Air-liquid interface cultures represent a valid tool for reproducing *in vitro* the typical aspects of the respiratory tract. In this configuration, cells can form a pseudostratified epithelium and differentiate towards a mucociliary phenotype better resembling *in vivo* conditions [39]. Calu-3 cells are considered as the gold standard of ALI cultures since under these culture conditions they express tight junctions, show high TEER values and secrete mucus [40,41]. In this study, we used the 3D culture model with Calu-3 cells, and monolayer formation was confirmed by tight junction staining visualized with confocal laser scanning microscopy as well as alcian blue staining of the mucus layer visualized with fluorescence microscopy (Supplementary Fig. 1). Due to their ability to secrete mucus under ALI conditions, Calu-3 cells represent a good model to investigate the mucus penetration of nanocarriers [42]. Calu-3 monolayers were stained with AF488-wheat germ agglutinin 24 h after transfection with AF647-siRNA/VIPER polyplexes, mounted on glass slides and directly analyzed by confocal microscopy without fixing. As it can be observed in the 3D reconstruction of Fig. 4(A–B), green fluorescence represents the mucus layer, while red dots correspond to the labeled siRNA penetrating through the mucus layer. Polyplexes efficiently diffused through the mucus layer and reached the underlying cell layer. To confirm the cellular internalization of the polyplexes after mucus penetration, an additional staining of the Calu-3 monolayer was performed to visualize cellular nuclei (blue), cytoskeleton (green) and AF647-labeled siRNA. As shown in Fig. 4(C–D), VIPER polyplexes, after overcoming the mucus layer, delivered siRNA to the underlying cells, confirming the potential of this polymer as delivery system in a challenging environment such as the respiratory tract.

Although the uptake of polyplexes was confirmed, its activity in the ALI culture model was still to be investigated. The activity of the polyplexes was studied by measuring the downregulation of the house-keeping gene GAPDH 24 h after transfection as previously described. In line with the 2D culture experiments, VIPER performed best, reaching about 75% downregulation of GAPDH expression (Fig. 4F). PEI showed similar results to lipofectamine, with about 40% reduction in GAPDH

expression besides potential off-target related upregulation of gene expression as reflected by the samples transfected with the negative control siRNA (siNC) [43]. This study confirmed the efficient delivery of siRNA to the Calu-3 monolayer by VIPER in a sophisticated culture system, which more closely mimics the *in vivo* conditions. In contrast, PEI polyplexes and Lipofectamine lipoplexes showed decreased efficacy (Supplementary Fig. 3) which can be understood as a result of hampered diffusion and “stickiness” in mucus caused by larger particles sizes and higher zeta potentials of PEI complexes than VIPER complexes. This observation is in line with the reported role of particle size in mucus diffusion [44].

3.6. siRNA/VIPER polyplex activity against wild-type SARS-CoV-2 on Calu-3 cells grown at ALI

After confirming the knockdown activity of siRNA/VIPER polyplexes in ALI cultures, we studied their activity against SARS-CoV-2 virus. The ACE-2 receptor is used by SARS-CoV-2 to infect human lung epithelial cells [45]. Since mouse ACE-2 does not bind efficiently to SARS-CoV-2, alternative *ex vivo* and *in vivo* models need to be considered for studying the activity of antiviral COVID drugs [46]. Although genetically engineered mouse models have been developed, they often present limitations in terms of accessibility. Therefore, the development of suitable *in vitro* and *ex vivo* models is critical for evaluating new antiviral candidates. Once cultured under ALI conditions, Calu-3 cells are known to express the ACE-2 receptor on the apical side, making them a suitable model for SARS-CoV-2 infection studies [39]. To confirm the expression of ACE-2 receptor by differentiated Calu-3 cells, cryosections of Calu-3 cells grown at ALI were prepared and stained with a goat anti-human ACE-2 antibody (magenta) and counterstained with DAPI (blue) (Fig. 5B). On the apical side, a strong signal was detected for the sections treated with the anti-ACE-2 primary antibody. On the contrary, no signal could be observed for control sections stained only with the secondary antibody (Fig. 5A). The staining of the receptor was homogeneous on the apical side of the monolayer while no signal could be detected on the basolateral side of the cells.

After confirming the presence of the ACE-2 receptor on the apical side of Calu-3 monolayer cells and therefore validating its suitability as infection model for SARS-CoV-2, cells were transfected with VIPER/siRNA polyplexes 6 h before infection with wild-type SARS-CoV-2 virus and readout performed after additional 24 h. The prophylactic siRNA application was established based on the observation that an early therapy start might be crucial for antiviral efficacy [12]. The siRNA sequence chosen for blocking the viral replication was described in a recently published work. The selected siRNA sequence targets a highly conserved region of the ORF1, and it was shown to efficiently inhibit the replication of the virus. ORF1 is a highly conserved region, suggesting a

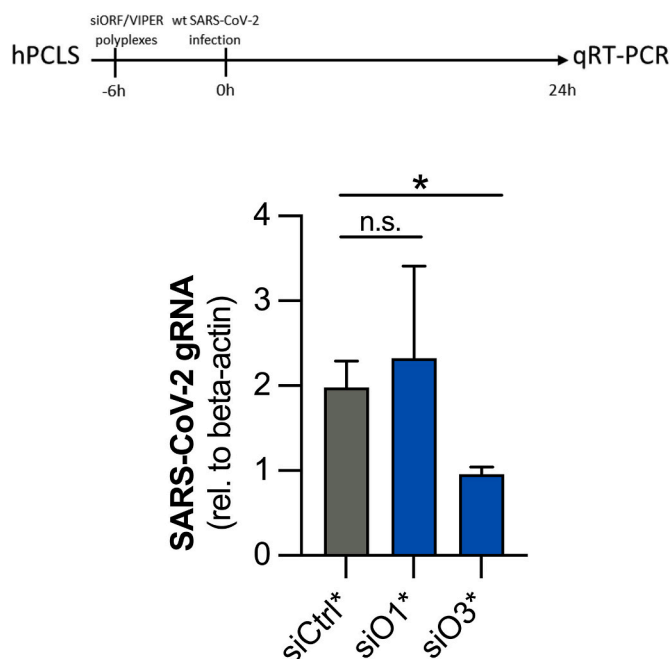


Fig. 6. Evaluation of siRNA/VIPER polyplexes against wild-type SARS-CoV-2 in human PCLS. PCLS were transfected with chemically modified versions of SARS-CoV-2 specific and luciferase control siRNA (see Table 1) formulated as VIPER polyplexes 6 h before infection with wild-type SARS-CoV-2 (MOI 1). The readout was performed 24 h after infection via qRT-PCR. Significant differences ($*p = 0.019$) were observed between the treatment with the unrelated luciferase vs. the O3* siRNA sequences. Data points indicate mean \pm SEM ($n = 3$).

limited likelihood of escape mutations that could make the virus resistant to therapy [12]. Based on our previous studies, we tested two different siRNA sequences targeting ORF1, O1 and O3. Polyplexes prepared with these sequences showed comparable characterization parameters to the siRNA sequence used for characterization and *in vitro* 2D activity experiments (Supplementary Table 1).

Indeed, infected ALI cells replicated SARS-CoV-2 at high levels, reaching extents that are only found in lungs of COVID-19 patients [47]. However, such high levels were only observed in cells that had received the control siRNA or which were only infected (Fig. 5C), while siORF1/VIPER polyplexes achieved a 50% and 75% reduction, for O1 and O3 respectively, of viral replication in comparison to the control groups, confirming the specific activity of the polyplexes against SARS-CoV-2. Most importantly, this study confirmed the activity of siRNA/VIPER polyplexes against SARS-CoV-2 in a relevant *in vitro* model incorporating the presence of mucus, which is one of the main barriers limiting the delivery of polyplexes to target cells in the respiratory tract.

3.7. Ex vivo activity in human precision-cut lung slices (PCLS)

Human PCLS are complex *ex vivo* 3D tissue culture models that closely mimic the anatomy and physiology of the lung. By maintaining the 3D architecture as well as the cellular diversity found in the lung, they represent a highly relevant model closing the translational gap between *in vitro* and *in vivo* models to study respiratory viruses and to evaluate siRNA delivery to the lung [23,48]. Previous studies confirmed their suitability as models for viral infections [49] as well as for testing the activity of siRNA-based formulations [50].

After titrating SARS-CoV-2 infection in PCLS (Supplementary Fig. 3), the activity of siORF/VIPER polyplexes was tested in a prophylactic setup resembling the one described in the ALI model above. Infection with 1.0 MOI was performed 6 h after polyplex transfection. qRT-PCR was performed 24 h after infection. In this experiment, chemically modified siRNA sequences of O1 and O3, namely O1* and

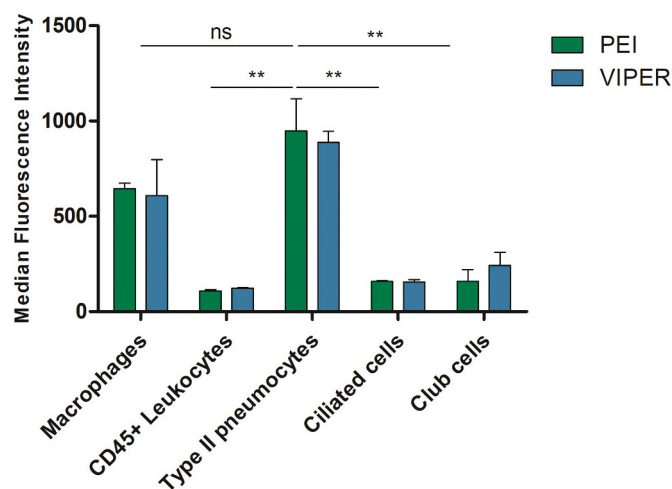


Fig. 7. *In vivo* siRNA/VIPER polyplexes distribution in lung epithelial cells. BALB/c mice were intratracheally administered with 2 nmol AF647-siRNA complexed with either VIPER or PEI polymers. Negative control consisted of animals that received 5% glucose only. Cellular uptake of VIPER and PEI polyplexes in different lung cell populations was quantified by flow cytometry. One-Way ANOVA, ns = not significant, $*p < 0.05$, $**p < 0.01$.

O3*, were used. Chemical modification of siRNA is a common practice to improve its stability, which becomes particularly relevant in a clinical setup [13]. Therefore, siRNA sequences were modified with the same modification pattern chosen for the recently approved Lumasiran [51]. Considering that the hPCLS model contains a variety of cell types and closely mimics *in vivo* condition, we decided to use the chemically modified siRNA for testing siRNA/VIPER polyplexes in 3D human lung explants. As shown in Supplementary Table 1, polyplexes prepared with the modified siRNA showed comparable characterization parameters to the ones prepared with the unmodified version. The results confirmed an siRNA-mediated decrease of viral replication of about 50% for O3* in comparison to the negative control. While the titration of the SARS-CoV-2 MOI amount in PCLS reflected a clear picture and confirmed infectability and dose-response in explanted human lung tissue (Supplementary Fig. 3), the additional parameter of transfection introduced increased variability. While, to the best of our knowledge, we are the first to report SARS-CoV-2 infection and therapeutic siRNA transfection in PCLS, we can only compare our results to PCLS transfections where endogenous genes were silenced. Ruigrok et al. reported approximately 50% gene silencing of GAPDH in PCLS [50]. However, we decided to silence viral factors rather than host factors with siRNA to avoid potential side effects. Therefore, our results of 50–75% gene silencing of coronaviral RNA levels in two different advanced models for SARS-CoV-2 infection emphasize the relevance of our approach as a promising therapy for the treatment of viral infections, particularly for COVID-19 (Fig. 6).

3.8. In vivo delivery of polyplexes

Epithelial cells are considered the main site for SARS-CoV-2 replication in the lungs [52]. Therefore, BALB/c mice were intratracheally administered with 2 nmol of VIPER as well as PEI polyplexes loaded with AF647-labeled siRNA to further assess pulmonary delivery of siRNA/VIPER polyplexes to epithelial cells. Two days after administration, bronchoalveolar lavage fluid (BALF) and blood were collected, while lungs were further processed to obtain a single cell suspension. Lung cells were counterstained with specific markers to identify different cellular populations present in the lung and to consequently understand the fate of polyplexes after pulmonary administration. As it can be observed in Fig. 7, both siRNA/PEI and siRNA/VIPER polyplexes were found mainly in two cellular subsets: type II pneumocytes and

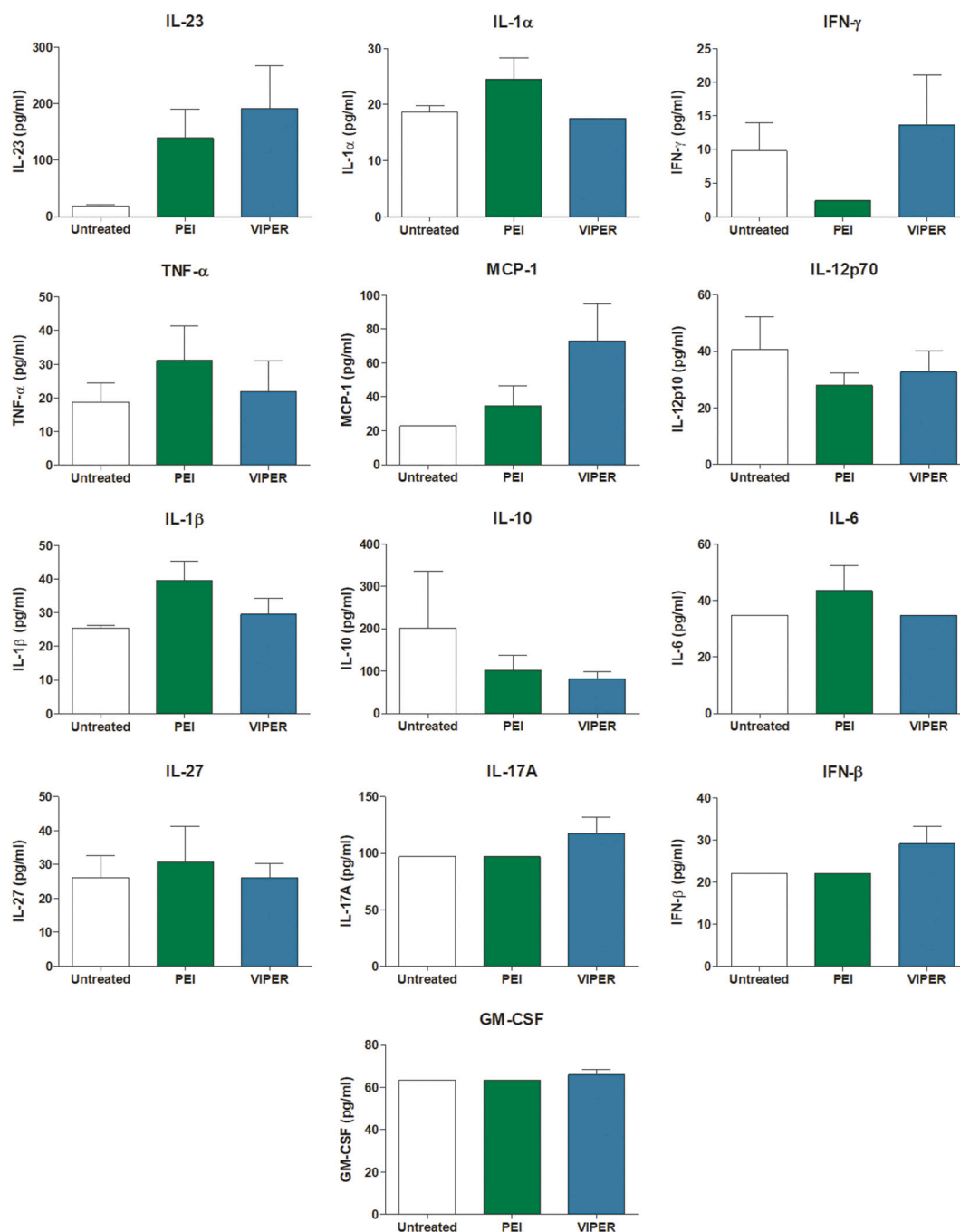


Fig. 8. *In vivo* cytokines release was measured in bronchoalveolar lavage fluid (BALF) by LEGENDplex ELISA technique. Values are given in pg/ml as mean \pm SEM ($n = 4$). Value below detection limit were set as the value corresponding to the minimum detection limit. One-Way ANOVA, only non-significant differences were observed.

macrophages. This experiment confirmed the delivery of siRNA to one of the main sites of viral replication - epithelial cells. Additionally, the cellular uptake observed in type II pneumocytes was surprisingly higher than the one observed in macrophages. Alveolar macrophages represent the first line cellular defense in the deep lung against foreign particulates, and their phagocytic activity could result in clearance of the administered polyplexes [53]. The ability to circumvent total macrophage clearance could be explained by the physicochemical characteristics of the formulation. Both PEI and VIPER polyplexes show sizes below 100 nm, while macrophages are known to most efficiently take up particles with sizes above 200 nm [54]. Additionally, the large surface area covered by type II pneumocytes as well as the corona of adsorbed

biomolecules [55] could favor the contact with the aerosolized polyplexes. Ultimately, the increased uptake of polyplexes by type II pneumocytes and in ciliated and club cells strengthens the rationale for using VIPER polymer for the delivery of siRNA to target the sites of viral replication in the lung [56,57]. Both VIPER and PEI polyplexes efficiently reached type II pneumocytes, ciliated and club cells, although no significant differences were observed between both nanocarriers. The aim of this experiment is a qualitative analysis of which cell types are passively targeted in the lung rather than a quantitative assessment of *in vivo* efficacy. In a previous study of ours [20], we demonstrated that VIPER polyplexes can outperform PEI polyplexes in terms of gene silencing *in vivo*. The current study together with our previous finding

confirms the potential of VIPER polyplexes as potential delivery system for siRNA against SARS-CoV-2 in the lung.

An important factor to be taken into consideration when studying *in vivo* delivery is the proinflammatory effect in response to the i.t. administration of polyplexes. Both PEI and VIPER are positively charged polymers that could trigger an inflammatory response in the lung [58,59]. Therefore, BALF and serum were analyzed with a LEGENDplex ELISA (BioLegend, San Diego, CA, USA) for inflammatory markers. As it can be observed in Figs. 8, 13 different inflammatory cytokines were analyzed simultaneously to detect any proinflammatory effects. Only two cytokines showed an increase after i.t administration of polyplexes; namely IL-23 and MCP-1, which act as monocyte chemoattractant and T_H17 expander, respectively. However, cytokine production was limited and not statistically significant. A previous study by Beyerle et al. showed that PEI-PEG polyplexes can induce a 9-fold increase of MCP-1 production in BALF in comparison to the control animals three days after intratracheal administration [59]. On the contrary, VIPER polyplexes induced only a 3-fold increase of MCP-1 expression in comparison to the control group which was not statistically significant. Furthermore, the proinflammatory effects following polyplexes administration were also analyzed in serum, to exclude systemic side effect (Supplementary Fig. 4). Out of the 13 cytokines tested, a slight increase was observed only for IL-1 α and IFN- β , 3-fold and 2-fold the control groups respectively. In line with the results from BALF analysis, no significant production of inflammatory cytokines was observed in serum.

4. Conclusion

In this study, we present a formulation for pulmonary delivery of siRNA for the treatment of respiratory viral infection with a focus on SARS-CoV-2. Our present works demonstrates the ability of the block copolymer VIPER to form polyplexes with optimal properties for pulmonary administration, as well as improved stability in the challenging environment typical for the lungs compared to PEI polyplexes. siRNA/VIPER polyplexes reached lung epithelial cells *in vitro* and *in vivo* and penetrated through the mucus layer typical of the airways in an air-liquid interface 3D culture model. Additionally, polyplexes showed good tolerability both *in vitro* and *in vivo*. The activity against SARS-CoV-2 was confirmed both *in vitro* in a 3D air-liquid interface cell culture model and *ex vivo* in 3D explants from human lungs. Collectively, these findings based on *in vitro* cell culture models, *ex vivo* human lung tissues and an *in vivo* animal model demonstrate the ability of siRNA/VIPER polyplexes to reach lung epithelial cells, the main site of viral replication in the lungs, and to suppress viral replication in mucus-covered cells as well as in human lung tissue. In conclusion, this study confirms the potential of siRNA-based therapies as antivirals and offers a new treatment option to tackle SARS-CoV-2 infection.

Credit author statement

Domizia Baldassi: Investigation, Methodology, Validation, Formal analysis, Writing - Original Draft, Visualization. Shubhankar Ambike: Investigation, Methodology, Formal analysis, Writing - Original Draft. Martin Feuerherd: Investigation, Methodology, Formal analysis. Cho-Chin Cheng: Investigation, Methodology, Formal analysis. David J Peeler: Investigation, Methodology, Formal analysis, Writing - Review & Editing. Daniel P Feldmann: Investigation, Methodology, Formal analysis, Writing - Review & Editing. Diana Leidy Porras-Gonzalez: Investigation. Xin Wei: Investigation. Lea-Adriana Keller: Investigation, Methodology, Formal analysis. Nikolaus Kneidinger: Resources. Mircea Gabriel Stoleriu: Resources. Andreas Popp: Methodology, Supervision. Gerald Burgstaller: Methodology, Resources, Funding Acquisition, Supervision. Suzie H Pun: Conceptualization, Methodology, Resources, Funding Acquisition, Supervision, Writing - Review & Editing, Project Administration. Thomas Michler: Conceptualization, Methodology, Resources, Funding Acquisition, Supervision, Writing - Review & Editing,

Project Administration. Olivia M Merkel: Conceptualization, Methodology, Resources, Funding Acquisition, Supervision, Writing - Review & Editing, Project Administration.

Declaration of Competing Interest

T.M. is an *ad hoc* advisor for VIR Biotechnology and received research grants by Alnylam Pharmaceuticals and Gilead Sciences. M.F. is a consultant for Dr. Hönle AG. O.M.M. is a consultant for AbbVie Deutschland GmbH, for PARI Pharma GmbH and an advisory board member for Coriolis Pharma GmbH. L.A.K. and A.P. are employees of AbbVie and may own AbbVie stock.

Acknowledgements

The authors thank Prof. Dr. Ulrike Protzer for general support such as providing the *wildtype* SARS-CoV-2 virus. We gratefully acknowledge the provision of human biomaterial and clinical data from the CPC-M bioArchive and its partners at the Asklepios Biobank Gauting, the Klinikum der Universität München and the Ludwig-Maximilians-Universität München. The Core Facility Flow Cytometry at the Biomedical Center, LMU Munich is gratefully acknowledged. Funding by the Bavarian State Government for Förderprogramm Corona-Forschung (to T.M.), by the Volkswagen Foundation (to O.M.M., T.M., G.B.), by the European Research Council [ERC-StG 637830 to O.M.M.], by the National Institute of Health (grant numbers 1R01CA257563 and 2R01NS064404 to S.H.P.) and by the German Academic Exchange Service (DAAD to S.A.) are gratefully acknowledged.

Appendix A. Supplementary data

Supplementary data to this article can be found online at <https://doi.org/10.1016/j.jconrel.2022.03.051>.

References

- [1] World Health Organization. <https://covid19.who.int/>, 2021. <https://covid19.who.int/>.
- [2] N.H.L. Leung, Transmissibility and transmission of respiratory viruses, *Nat. Rev. Microbiol.* 19 (2021) 528–545, <https://doi.org/10.1038/s41579-021-00535-6>.
- [3] J.P. Bridges, E.K. Vadar, H. Huang, R.J. Mason, Respiratory epithelial cell responses to SARS-CoV-2 in COVID-19, *Thorax*. (2021), <https://doi.org/10.1136/thoraxjnl-2021-217561>
- [4] W. Guan, Z. Ni, Y. Hu, W. Liang, C. Ou, J. He, L. Liu, H. Shan, C. Lei, D.S.C. Hui, B. Du, L. Li, G. Zeng, K.-Y. Yuen, R. Chen, C. Tang, T. Wang, P. Chen, J. Xiang, S. Li, J. Wang, Z. Liang, Y. Peng, L. Wei, Y. Liu, Y. Hu, P. Peng, J. Wang, J. Liu, Z. Chen, G. Li, Z. Zheng, S. Qiu, J. Luo, C. Ye, S. Zhu, N. Zhong, Clinical Characteristics of Coronavirus Disease 2019 in China, *N. Engl. J. Med.* 382 (2020) 1708–1720, <https://doi.org/10.1056/nejmoa2002032>.
- [5] FDA. <https://www.fda.gov/emergency-preparedness-and-response/coronavirus-disease-2019-covid-19/covid-19-vaccines>, 2021.
- [6] EMA. <https://www.ema.europa.eu/en/human-regulatory/overview/public-health-threats/coronavirus-disease-covid-19/treatments-vaccines/covid-19-vaccines>, 2021.
- [7] Y. Wang, D. Zhang, G. Du, R. Du, J. Zhao, Y. Jin, S. Fu, L. Gao, Z. Cheng, Q. Lu, Y. Hu, G. Luo, K. Wang, Y. Lu, H. Li, S. Wang, S. Ruan, C. Yang, C. Mei, Y. Wang, D. Ding, F. Wu, X. Tang, X. Ye, Y. Ye, B. Liu, J. Yang, W. Yin, A. Wang, G. Fan, F. Zhou, Z. Liu, X. Gu, J. Xu, L. Shang, Y. Zhang, L. Cao, T. Guo, Y. Wan, H. Qin, Y. Jiang, T. Jaki, F.G. Hayden, P.W. Horby, B. Cao, C. Wang, Remdesivir in adults with severe COVID-19: a randomised, double-blind, placebo-controlled, multicentre trial, *Lancet*. 395 (2020) 1569–1578, [https://doi.org/10.1016/S0140-6736\(20\)31022-9](https://doi.org/10.1016/S0140-6736(20)31022-9).
- [8] Pfizer press release. <https://www.pfizer.com/news/press-release/press-release-detail/pfizer-announces-additional-phase-23-study-results>, 2021.
- [9] A. Jayk Bernal, M.M. Gomes da Silva, D.B. Musungaie, E. Kovalchuk, A. Gonzalez, V. Delos Reyes, A. Martín-Quiros, Y. Caraco, A. Williams-Diaz, M.L. Brown, J. Du, A. Pedley, C. Assaid, J. Strizki, J.A. Grobler, H.H. Shamsuddin, R. Tipping, H. Wan, A. Paschke, J.R. Butterton, M.G. Johnson, C. De Anda, MOVE-OUT study group, Molnupiravir for Oral treatment of Covid-19 in nonhospitalized patients, *N. Engl. J. Med.* (2021) 1–12, <https://doi.org/10.1056/NEJMoa2116044>.
- [10] P. V'kovski, A. Kratzel, S. Steiner, H. Stalder, V. Thiel, Coronavirus biology and replication: implications for SARS-CoV-2, *Nat. Rev. Microbiol.* 19 (2021) 155–170, <https://doi.org/10.1038/s41579-020-00468-6>.

- [11] A. Levanova, M.M. Poranen, RNA interference as a prospective tool for the control of human viral infections, *Front. Microbiol.* 9 (2018), <https://doi.org/10.3389/fmicb.2018.02151>.
- [12] S. Ambike, C. Cheng, M. Feuerherd, S. Velkov, D. Baldassi, S.Q. Afridi, D. Porrason-gonzalez, X. Wei, P. Hagen, N. Kneidinger, M.G. Stoleriu, V. Grass, G. Burgstaller, A. Pichlmair, O.M. Merkel, C. Ko, T. Michler, Targeting genomic SARS-CoV-2 RNA with siRNAs allows efficient inhibition of viral replication and spread, *Nucleic Acids Res.* (2021) 1–17, <https://doi.org/10.1093/nar/gkab1248>.
- [13] A. Mehta, T. Michler, O.M. Merkel, siRNA therapeutics against respiratory viral infections—what have we learned for potential COVID-19 therapies? *Adv. Healthc. Mater.* 10 (2021) <https://doi.org/10.1002/adhm.202001650>.
- [14] L. Azzi, D.D. Gasperina, G. Veronesi, M. Shallak, G. Ietto, D. Iovino, A. Baj, F. Gianfagna, V. Maurino, D. Focosi, F. Maggi, M. Ferrario, F. Dentali, G. Carcano, A. Tagliabue, S. Maf, S. Accolla, G. Forlani, Mucosal immune response in BNT162b2 COVID-19 vaccine recipients, *EBioMedicine.* 75 (2022), 103788, <https://doi.org/10.1016/j.ebiom.2021.103788>.
- [15] R. Kandil, O.M. Merkel, Pulmonary delivery of siRNA as a novel treatment for lung diseases, *Ther. Deliv.* 10 (2019) 203–206, <https://doi.org/10.4155/tde-2019-0009>.
- [16] O.M. Merkel, I. Rubinstein, T. Kissel, siRNA delivery to the lung: What's new? *Adv. Drug Deliv. Rev.* 75 (2014) 112–128, <https://doi.org/10.1016/j.addr.2014.05.018>.
- [17] D. Cipolla, I. Gonda, H.K. Chan, Liposomal formulations for inhalation, *Ther. Deliv.* 4 (2013) 1047–1072, <https://doi.org/10.4155/tde.13.71>.
- [18] T.W.M. Keil, C. Zimmermann, D. Baldassi, F. Adams, W. Friess, A. Mehta, O. M. Merkel, Impact of crystalline and amorphous matrices on successful spray drying of siRNA Polyplexes for inhalation of Nano-in-microparticles, *Adv. Ther.* 4 (2021) 1–15, <https://doi.org/10.1002/adtp.202100073>.
- [19] Y. Cheng, R.C. Yumul, S.H. Pun, Virus-inspired polymer for efficient in vitro and in vivo gene delivery, *Angew. Chem. Int. Ed.* 55 (2016) 12013–12017, <https://doi.org/10.1002/anie.201605958>.
- [20] D.P. Feldmann, Y. Cheng, R. Kandil, Y. Xie, M. Mohammadi, H. Harz, A. Sharma, D. J. Peeler, A. Moszczynska, H. Leonhardt, S.H. Pun, O.M. Merkel, In vitro and in vivo delivery of siRNA via VIPER polymer system to lung cells, *J. Control. Release* 276 (2018) 50–58, <https://doi.org/10.1016/j.jconrel.2018.02.017>.
- [21] I.M.S. Degors, C. Wang, Z.U. Rehman, I.S. Zuhorn, Carriers break barriers in drug delivery: endocytosis and endosomal escape of gene delivery vectors, *Acc. Chem. Res.* 52 (2019) 1750–1760, <https://doi.org/10.1021/acs.accounts.9b00177>.
- [22] D. Baldassi, B. Gabold, O.M. Merkel, Air–liquid Interface cultures of the healthy and diseased human respiratory tract: promises, challenges, and future directions, *Adv. NanoBiomed Res.* 1 (2021) 2000111, <https://doi.org/10.1002/anbr.202000111>.
- [23] G. Liu, C. Betts, D.M. Cunoosamy, P.M. Åberg, J.J. Hornberg, K.B. Sivars, T. S. Cohen, Use of precision cut lung slices as a translational model for the study of lung biology, *Respir. Res.* 20 (2019) 1–14, <https://doi.org/10.1186/s12931-019-1131-x>.
- [24] D.J. Peeler, S.N. Thai, Y. Cheng, P.J. Horner, D.L. Sellers, S.H. Pun, pH-sensitive polymer micelles provide selective and potentiated lytic capacity to venom peptides for effective intracellular delivery, *Biomaterials.* 192 (2019) 235–244, <https://doi.org/10.1016/j.biomaterials.2018.11.004>.
- [25] Y. Xie, N.H. Kim, V. Nadithe, D. Schalk, A. Thakur, A. Kılıç, L.G. Lum, D.J. P. Bassett, O.M. Merkel, Targeted delivery of siRNA to activated T cells via transferrin-polyethyleneimine (Tf-PEI) as a potential therapy of asthma, *J. Control. Release* 229 (2016) 120–129, <https://doi.org/10.1016/j.jconrel.2016.03.029>.
- [26] O.M. Merkel, D. Librizzi, A. Pfestroff, T. Schurrat, M. Béhé, T. Kissel, In vivo SPECT and real-time gamma camera imaging of biodistribution and pharmacokinetics of siRNA delivery using an optimized radiolabeling and purification procedure, *Bioconjug. Chem.* 20 (2009) 174–182, <https://doi.org/10.1021/bc800408g>.
- [27] M. Gerckens, H.N. Alsafadi, D.E. Wagner, M. Lindner, G. Burgstaller, M. Königshoff, Generation of human 3D lung tissue cultures (3D-LTCs) for disease modeling, *J. Vis. Exp.* (2019) 1–8, <https://doi.org/10.3791/58437>.
- [28] H.N. Alsafadi, C.A. Staab-Weijnitz, M. Lehmann, M. Lindner, B. Peschel, M. Königshoff, D.E. Wagner, An ex vivo model to induce early fibrosis-like changes in human precision-cut lung slices, *Am. J. Phys. Lung Cell. Mol. Phys.* 312 (2017) L896–L902, <https://doi.org/10.1152/ajplung.00084.2017>.
- [29] O.M. Merkel, L.M. Marsh, H. Garn, T. Kissel, Flow cytometry-based cell type-specific assessment of target regulation by pulmonary siRNA delivery, *Methods Mol. Biol.* 948 (2013) 1–7, https://doi.org/10.1007/978-1-62703-140-0_18.
- [30] O.M. Merkel, A. Beyerle, D. Librizzi, A. Pfestroff, T.M. Behr, B. Sproat, P.J. Barth, T. Kissel, Nonviral siRNA delivery to the lung: investigation of PEG-PEI polyplexes and their in vivo performance, *Mol. Pharm.* 6 (2009) 1246–1260, <https://doi.org/10.1021/mp900107v>.
- [31] S. Pramanik, S. Mohanto, R. Manne, R.R. Rajendran, A. Deepak, S.J. Edapully, T. Patil, O. Katari, Nanoparticle-based drug delivery system: the magic bullet for the treatment of chronic pulmonary diseases, *Mol. Pharm.* 18 (2021) 3671–3718, <https://doi.org/10.1021/acs.molpharmaceut.1c00491>.
- [32] M.A. Tomeh, X. Zhao, Recent advances in microfluidics for the preparation of drug and gene delivery systems, *Mol. Pharm.* 17 (2020) 4421–4434, <https://doi.org/10.1021/acs.molpharmaceut.0c00913>.
- [33] K. Abstiens, A.M. Goepferich, Microfluidic manufacturing improves polydispersity of multicomponent polymeric nanoparticles, *J. Drug Deliv. Sci. Technol.* 49 (2019) 433–439, <https://doi.org/10.1016/j.jddst.2018.12.009>.
- [34] D.P. Feldmann, O.M. Merkel, The advantages of pulmonary delivery of therapeutic siRNA, *Ther. Deliv.* 7 (2016) 117–138, <https://doi.org/10.4155/tde.15.92>.
- [35] G.A. Duncan, J. Jung, J. Hanes, J.S. Suk, The mucus barrier to inhaled gene therapy, *Mol. Ther.* 24 (2016) 2043–2053, <https://doi.org/10.1038/mt.2016.182>.
- [36] H. Wei, L.R. Volpatti, D.L. Sellers, D.O. Maris, I.W. Andrews, A.S. Hemphill, L. W. Chan, D.S.H. Chu, P.J. Horner, S.H. Pun, Dual responsive, stabilized nanoparticles for efficient in vivo plasmid delivery, *Angew. Chem. Int. Ed.* 52 (2013) 5377–5381, <https://doi.org/10.1002/anie.201301896>.
- [37] B.A. Paray, A. Ahmad, J.M. Khan, F. Taufiq, A. Pathan, A. Malik, M.Z. Ahmed, The role of the multifunctional antimicrobial peptide melittin in gene delivery, *Drug Discov. Today* 26 (2021) 1053–1059, <https://doi.org/10.1016/j.drudis.2021.01.004>.
- [38] D.J. Peeler, A. Yen, N. Luera, P.S. Stayton, S.H. Pun, Lytic Polyplex vaccines enhance antigen-specific cytotoxic T cell response through induction of local cell death, *Adv. Ther.* 4 (2021) 1–11, <https://doi.org/10.1002/adtp.202100005>.
- [39] N. Heinen, M. Klöhn, E. Steinmann, S. Pfander, In vitro lung models and their application to study sars-cov-2 pathogenesis and disease, *Viruses.* 13 (2021), <https://doi.org/10.3390/v13050792>.
- [40] C.I. Grainger, L.L. Greenwell, D.J. Lockley, G.P. Martin, B. Forbes, Culture of Calu-3 cells at the air Interface provides a representative model of the airway epithelial barrier, *Pharm. Res.* 23 (2006) 1482–1490, <https://doi.org/10.1007/s11095-006-0255-0>.
- [41] H.M. Braakhuis, R. He, R.J. Vandebriel, E.R. Gremmer, E. Zwart, J.P. Vermeulen, P. Fokkens, J. Boere, I. Gosens, F.R. Cassee, An air-liquid interface bronchial epithelial model for realistic, repeated inhalation exposure to airborne particles for toxicity testing, *J. Vis. Exp.* 2020 (2020) 1–10, <https://doi.org/10.3791/61210>.
- [42] S. Mura, H. Hillaireau, J. Nicolas, S. Kerdine-Römer, B. Le Droumaguet, C. Deloménie, V. Nicolas, M. Pallardy, N. Tsapis, E. Fattal, Biodegradable nanoparticles meet the bronchial airway barrier: how surface properties affect their interaction with mucus and epithelial cells, *Biomacromolecules.* 12 (2011) 4136–4143, <https://doi.org/10.1021/bm201226x>.
- [43] O.M. Merkel, A. Beyerle, B.M. Beckmann, M. Zheng, R.K. Hartmann, T. Stöger, T. H. Kissel, Polymer-related off-target effects in non-viral siRNA delivery, *Biomaterials.* 32 (2011) 2388–2398, <https://doi.org/10.1016/j.biomaterials.2010.11.081>.
- [44] X. Murgia, P. Pawelczyk, U.F. Schaefer, C. Wagner, N. Willenbacher, C.M. Lehr, Size-limited penetration of nanoparticles into porcine respiratory mucus after aerosol deposition, *Biomacromolecules.* 17 (2016) 1536–1542, <https://doi.org/10.1021/acs.biomac.6b00164>.
- [45] M. Hoffmann, H. Kleine-Weber, S. Schroeder, N. Krüger, T. Herrler, S. Erichsen, T. S. Schiergens, G. Herrler, N.H. Wu, A. Nitsche, M.A. Müller, C. Drosten, S. Pöhlmann, SARS-CoV-2 cell entry depends on ACE2 and TMPRSS2 and is blocked by a clinically proven protease inhibitor, *Cell.* 181 (2020) 271–280.e8, <https://doi.org/10.1016/j.cell.2020.02.052>.
- [46] H. Jia, X. Yue, E. Lazartigues, ACE2 mouse models: a toolbox for cardiovascular and pulmonary research, *Nat. Commun.* 11 (2020), <https://doi.org/10.1038/s41467-020-18880-0>.
- [47] H.T. Puelles VG, M. Lütgehetmann, M.T. Lindenmeyer, J.P. Sperhake, M.N. Wong, L. Allweiss, S. Chilla, A. Heinemann, N. Wanner, S. Liu, F. Braun, S. Lu, S. Pfefferle, A.S. Schröder, C. Edler, O. Gross, M. Glatzel, D. Wichmann, T. Wüch, S. Kluge, K. Püeschel, M. Aepfelbacher, Multiorgan and renal tropism of SARS-CoV-2, *N. Engl. J. Med.* 383 (2020) 590–592, <https://doi.org/10.1056/NEJMc2011400>.
- [48] F. Viana, C.M. O’Kane, G.N. Schroeder, Precision-cut lung slices: a powerful ex vivo model to investigate respiratory infectious diseases, *Mol. Microbiol.* (2021) 1–11, <https://doi.org/10.1111/mmi.14817>.
- [49] M.C. Rosales Gerpe, J.P. van Vloten, L.A. Santry, J. de Jong, R.C. Mould, A. Pelin, J.C. Bell, B.W. Bridle, S.K. Wootton, Use of precision-cut lung slices as an ex vivo tool for evaluating viruses and viral vectors for gene and Oncolytic therapy, *Mol. Ther. - Methods Clin. Dev.* 10 (2018) 245–256, <https://doi.org/10.1016/j.omtm.2018.07.010>.
- [50] M.J.R. Ruigrok, J.L. Xian, H.W. Frijlink, B.N. Melgert, W.L.J. Hinrichs, P. Olinga, siRNA-mediated protein knockdown in precision-cut lung slices, *Eur. J. Pharm. Biopharm.* 133 (2018) 339–348, <https://doi.org/10.1016/j.ejpb.2018.11.005>.
- [51] D.J. Foster, C.R. Brown, S. Shaikh, C. Trapp, M.K. Schlegel, K. Qian, A. Sehgal, K. G. Rajeev, V. Jadhav, M. Manoharan, S. Kuchimanchi, M.A. Maier, S. Milstein, Advanced siRNA designs further improve in vivo performance of GalNAc-siRNA conjugates, *Mol. Ther.* 26 (2018) 708–717, <https://doi.org/10.1016/j.ymthe.2017.12.021>.
- [52] G. Ryu, H.W. Shin, Sars-cov-2 infection of airway epithelial cells, *Immune Netw.* 21 (2021) 1–16, <https://doi.org/10.4110/in.2021.21.e3>.
- [53] M. Kopf, C. Schneider, S.P. Nobs, The development and function of lung-resident macrophages and dendritic cells, *Nat. Immunol.* 16 (2015) 36–44, <https://doi.org/10.1038/ni.3052>.
- [54] T. Petithory, L. Pieuchot, L. Josien, A. Ponche, K. Anselme, L. Vonna, Size-dependent internalization efficiency of macrophages from adsorbed nanoparticle-based monolayers, *Nanomaterials.* 11 (2021), <https://doi.org/10.3390/nano11081963>.
- [55] B. Yin, C.K.W. Chan, S. Liu, H. Hong, S.H.D. Wong, L.K.C. Lee, L.W.C. Ho, L. Zhang, K.C.F. Leung, P.C.L. Choi, L. Bian, X.Y. Tian, M.N. Chan, C.H.J. Choi, Intrapulmonary cellular-level distribution of inhaled nanoparticles with defined functional groups and its correlations with protein Corona and inflammatory response, *ACS Nano* 13 (2019) 14048–14069, <https://doi.org/10.1021/acsnano.9b06424>.
- [56] S. Lukassen, R.L. Chua, T. Trefzer, N.C. Kahn, M.A. Schneider, T. Muley, H. Winter, M. Meister, C. Veith, A.W. Boots, B.P. Hennig, M. Kreuter, C. Conrad, R. Eils, SARS-CoV-2 receptor ACE 2 and TMPRSS 2 are primarily expressed in bronchial transient secretory cells, *EMBO J.* 39 (2020) 1–15, <https://doi.org/10.15252/embj.20105114>.
- [57] J. Liu, Y. Li, Q. Liu, Q. Yao, X. Wang, H. Zhang, R. Chen, L. Ren, J. Min, F. Deng, B. Yan, L. Liu, Z. Hu, M. Wang, Y. Zhou, SARS-CoV-2 cell tropism and multiorgan

- infection, *Cell Discov.* 7 (2021) 2–5, <https://doi.org/10.1038/s41421-021-00249-2>.
- [58] A. Beyerle, A. Braun, O. Merkel, F. Koch, T. Kissel, T. Stoeger, Comparative in vivo study of poly(ethylene imine)/siRNA complexes for pulmonary delivery in mice, *J. Control. Release* 151 (2011) 51–56, <https://doi.org/10.1016/j.jconrel.2010.12.017>.
- [59] A. Beyerle, A. Braun, A. Banerjee, N. Ercal, O. Eickelberg, T.H. Kissel, T. Stoeger, Inflammatory responses to pulmonary application of PEI-based siRNA nanocarriers in mice, *Biomaterials*. 32 (2011) 8694–8701, <https://doi.org/10.1016/j.biomaterials.2011.07.082>.